Cryogenics 51 (2011) 591–597

Contents lists available at SciVerse ScienceDirect

Cryogenics

journal homepage: www.elsevier.com/locate/cryogenics

The frequency dependent regenerator cold section and hot section positional reversal in a coaxial type thermoacoustic Stirling heat pump

Adhika Widyaparaga [a,e,*], Takao Koshimizu [b], Eiji Noda [a], Naoya Sakoda [c], Masamichi Kohno [a,d], Yasuyuki Takata [a,d]

[a] Department of Mechanical Engineering, Kyushu University, 744 Motooka, Nishi-ku, Fukuoka, Japan
[b] Department of Mechanical Engineering, Kitakyushu National College of Technology, 5-20-1 Shii, Kokuraminamiku, Kitakyushu, Japan
[c] International Research Centre for Hydrogen Energy, Kyushu University, 744 Motooka, Nishi-ku, Fukuoka, Japan
[d] International Institute for Carbon-Neutral Energy Research (I²CNER), Kyushu University, 744 Motooka, Nishi-ku, Fukuoka, Japan
[e] Department of Mechanical and Industrial Engineering, Gadjah Mada University, Jl. Grafika 2, Yogyakarta, Indonesia

ARTICLE INFO

Article history:
Received 22 March 2011
Received in revised form 16 August 2011
Accepted 4 September 2011
Available online 14 September 2011

Keywords:
Thermoacoustic
Coaxial
Travelling wave
Stirling heat pump

ABSTRACT

We have constructed and tested two travelling wave thermoacoustic heat pumps using a coaxial configuration with the regenerator positioned in the annulus. We discovered a frequency dependent positional reversal of the cold section and hot section of the regenerator within the test frequency range. By decomposing the measured pressure wave within the annulus, we obtained the positive (w_+) and negative (w_-) propagating travelling waves. It has been revealed the change of frequency is accompanied by a change in magnitudes of w_+ and w_- which is in part influenced by the presence of travelling wave attenuation through the regenerator. The resulting change of dominant travelling wave on a given end of the regenerator will then change the direction of thermoacoustic heat pumping at that end. This will alter the regenerator temperature distribution and may reverse the cold and hot sections of the regenerator. As the reversal does not require additional moving parts, merely a change in frequency, this feature in coaxial travelling wave devices has tremendous potential for applications which require both heating and cooling operation.

© 2011 Elsevier Ltd. All rights reserved.

1. Introduction

Most early work regarding thermoacoustic devices focused on standing wave thermoacoustic devices [1–3]. These standing wave devices involved an inherent irreversibility due to the required thermal delay for optimum operation, limiting the efficiency. Therefore, Ceperley [4] proposed to employ travelling wave thermoacoustic effects, instead of standing wave thermoacoustic effects, which do not require a thermal delay thus allowing higher efficiencies. Since in a travelling wave, the gas undergoes a thermodynamic cycle similar to a Stirling cycle, travelling wave thermoacoustic devices are often referred to as thermoacoustic Stirling devices.

The first thermoacoustic Stirling device was a loop type thermoacoustic Stirling engine built and tested by Yazaki et al. [5]. The presence of nonlinearities such as mass streaming, were found to reduce efficiency. This was remedied in the design of Backhaus and Swift [6], which was a thermoacoustic Stirling engine employing a loop design as well. The first thermoacoustic Stirling refrigeration device was also developed by Yazaki et al. [7] using a loop configuration.

While loop devices have been proven to work well, they seem somewhat unwieldy in regards to constructing a compact device. An alternative for a travelling wave device is a coaxial configuration. However, there have been only a few works regarding coaxial thermoacoustic devices. The first coaxial thermoacoustic device, while not explicitly termed, was the design by Poese et al. [8], a thermoacoustic Stirling heat pump intended as a cooler for an ice cream cabinet. A coaxial configuration was also developed and tested by Tijani and Spoelstra [9].

Interestingly, comparing the two coaxial devices in the studies above, the temperature gradients within the regenerators were reversed, resulting in opposite positions of the cold section and hot sections between the two studies. The regenerator section at the end of the device was the hot section for the device by Tijani and Spoelstra while Poese et al. obtained a cold section at the end. These studies used different operating frequencies and also employed different device dimensions which may have accounted for the difference in the temperature gradient sign within the regenerator.

* Corresponding author at: Department of Mechanical Engineering, Kyushu University, 744 Motooka, Nishi-ku, Fukuoka, Japan.
E-mail address: adhikayev@gmail.com (A. Widyaparaga).

0011-2275/$ - see front matter © 2011 Elsevier Ltd. All rights reserved.
doi:10.1016/j.cryogenics.2011.09.001

Nomenclature

r_h	hydraulic diameter (m)
κ	wavenumber (m^{-1})
t	time (s)
x	distance (m)
w	pressure wave (Pa)
w_a	pressure wave analytic signal (Pa)
SWR	standing wave ratio

Greek symbols

α	thermal diffusivity (m^2/s)
ω	angular velocity (rad/s)
τ	thermal relaxation time (s)
σ	1/SWR

Subscripts

regen	regenerator mesh
+	positive direction
−	negative direction

We have thus focused on the reversal of regenerator temperature gradient in our study. The objective of our study was to create a hot section and cold section positional reversal using a frequency change and investigate the mechanism of this reversal.

In addition, all the coaxial thermoacoustic device studies mentioned above have positioned the regenerator inside the inner tube. This is somewhat disadvantageous since the positioning of heat exchangers will not be in close proximity with the outer environment. Here, we have constructed travelling wave thermoacoustic heat pumps using a coaxial design employing a regenerator in the annulus as opposed to the inner tube, a configuration first developed by Biwa and Morii [10].

Being able to alter the position of the hot and cold section, and produce a reversal in a single thermoacoustic device will be important in the development of devices for applications requiring both cooler and heater operation, potentially allowing both cryocooling and superheating using a single device merely with an operating frequency change and without additional parts.

2. Apparatus and experiment

We have constructed two configurations of coaxial thermoacoustic heat pumps. Both configurations used air as a medium at atmospheric pressure and room temperature. We have designated the configurations as Configuration A and Configuration B.

The diagram of Configuration A is shown in Fig. 1. It consists of an outer acrylic tube with an inner diameter of 50 mm and wall thickness of 5 mm arranged concentrically with an inner acrylic tube with an outer diameter of 28 mm and wall thickness of 1 mm. The inner tube was of a length of 300 mm. A resonator of 508 mm was used corresponding to the half wave length for 340 Hz.

The regenerator was constructed of 230 sheets of stainless steel mesh with a mesh number of 150. The mesh sheets were stacked to a total regenerator length of 30 mm. The mesh openings had a hydraulic radius of 0.025 mm which is smaller than the thermal penetration depth for air within the tested frequency range.

It will be shown later that Configuration A features a good temperature drop for both low and high frequencies. However, the position of the regenerator was as such to cause difficulty in measuring the pressure wave at the further end of the regenerator. Therefore, for better understanding of the phenomenon, we have constructed a second configuration, Configuration B, with the position of the regenerator modified to allow positioning of pressure sensors measuring the pressure wave within the annulus on the T_2 side of the regenerator (Fig. 2). Configuration B uses a similar regenerator with the same dimensions and mesh specifications. The length of the inner tube remains the same 300 mm. However, the length of the resonator is slightly longer at 520 mm.

The apparatus setup for Configuration B is shown in Fig. 3. A Jordan JX-92S full range woofer was used as the acoustic driver. The signal was generated using an Agilent 33220A waveform generator

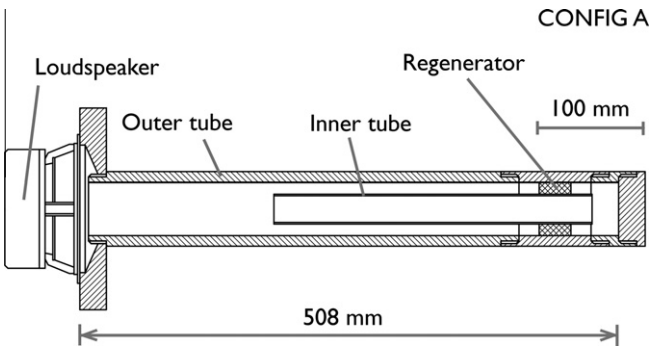

Fig. 1. Coaxial thermoacoustic heat pump Configuration A.

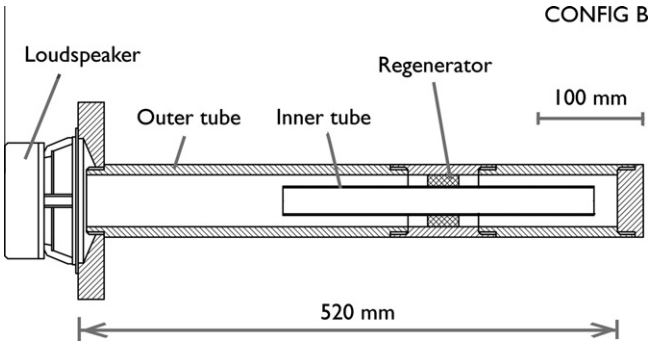

Fig. 2. Coaxial thermoacoustic heat pump Configuration B.

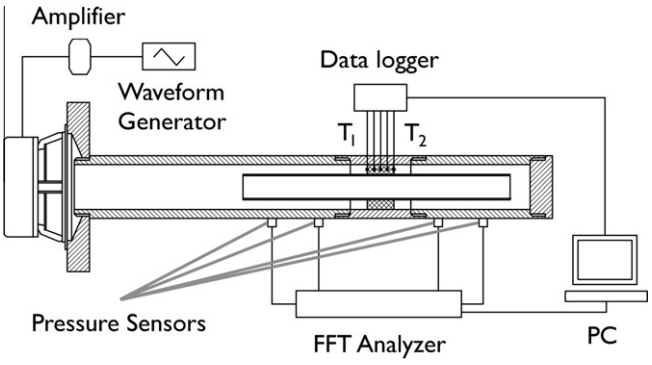

Fig. 3. Apparatus setup for Configuration B; thermocouple positions at the ends of the regenerator labeled T_1 and T_2 are displayed.

connected to a Yamaha P-1000S Amplifier. We have specified the thermocouples at the regenerator ends as T_1 located at the closer end facing toward the acoustic driver and T_2 located at the further end facing away from the acoustic driver. Three additional thermocouples were positioned within the regenerator as such so the five thermocouple positions are at regular intervals along the regenerator. Pressure measurements were conducted using PCB Piezotronics M102A05 pressure sensors positioned at the annulus. Temperature measurements were conducted using Type K thermocouples connected to an Agilent 34970A data acquisition unit. The apparatus setup for Configuration A is similar to Configuration B but without the presence of pressure measurements at the T_2 end of the regenerator.

Heat exchangers at the ends of the regenerator were not incorporated in the system since they would alter the original temperature distribution within the regenerator caused by the thermoacoustic effect of the positive and negative direction travelling waves. Without the presence of heat exchangers, the change of regenerator temperature distribution in relation to the change of frequency and magnitudes of the positive and negative direction travelling waves was more clearly observable, later proving important in obtaining the U-shaped temperature distribution described in Section 5.

The frequencies tested ranged from 100 Hz to 400 Hz. We have used input electric powers of 3 W and 38 W. The temperatures at the regenerator were recorded for a running time 60 min for 3 W and 10 min for 38 W. The pressure waves at the T_1 end and T_2 end (for Configuration B) were recorded with a sampling frequency of 50 kHz.

3. Thermal contact

In practice, the observed final thermoacoustic effect is the result of the combination of both the standing wave thermoacoustic effects and the travelling wave thermoacoustic effects [11]. The parameter $\omega\tau$ characterizes the thermal contact between the gas medium and the regenerator surfaces [12] which in turn describes the contribution of the travelling wave effect and standing wave effect to the energy conversion in the regenerator [13]. The thermal relaxation time τ is calculated by:

$$\tau = \frac{(2r_{h,\mathrm{regen}})^2}{2\alpha} \tag{1}$$

A value of $\omega\tau$ much smaller than π indicates a reversibility of the gas movement within the regenerator channels and gas temperature equating that of the regenerator surfaces thus is a suitable regime for the operation of travelling wave thermoacoustic devices. For the test range of 100–400 Hz, we obtain $\omega\tau$ of 0.04 for 100 Hz to 0.14 for 400 Hz. Both are much lower than π therefore the test range is favorable for travelling wave operation. These values of $\omega\tau$ would render standing wave thermoacoustic effects negligible [13].

4. Wave decomposition

As standing wave effects are negligible, the resulting temperature gradient within the regenerator will be due to the travelling wave effects. Since there is an observed sign change of regenerator temperature gradient, we must consider both the initiating travelling wave and a reflected travelling wave which compose the acoustic field within the regenerator instead of only taking into account the measured combined pressure wave. It is thus important to decompose the measured pressure wave into its positive and negative propagating components.

We have therefore conducted a spatial and temporal wave decomposition for the measured pressure wave at the annulus of T_1 side of the regenerator for Configuration A and for the measured pressure wave at the annulus of the T_1 and T_2 side for Configuration B.

The acoustic pressure wave can be expressed as [14]:

$$w(x,t) = A(\kappa x)\cos\omega t + B(\kappa x)\sin\omega t \tag{2}$$

where

$$A(\kappa x) = A_1\cos\kappa x + A_2\sin\kappa x \tag{3}$$

$$B(\kappa x) = B_1\cos\kappa x + B_2\sin\kappa x \tag{4}$$

As described by Bucher [14], using the Hilbert transform, the analytic signal describing the relative phase information of the wave is obtained:

$$w_a(x,t) = \{(A_1 - B_2) - i(A_2 + B_1)\}e^{i(\omega t+\kappa x)} + \{(A_1 + B_2) - i(-A_2 + B_1)\}e^{i(\omega t-\kappa x)} \tag{5}$$

The first term and second term of equation are the terms for the travelling waves propagating in the negative (w_-) and positive (w_+) directions respectively. By finding the coefficients A_1, A_2, B_1 and B_2, we can describe the waves separately:

$$w_-(x,t) = \{(A_1 - B_2) + i(-A_2 - B_1)\}e^{i(\omega t+\kappa x)} \tag{6}$$

$$w_+(x,t) = \{(A_1 + B_2) + i(A_2 - B_1)\}e^{i(\omega t-\kappa x)} \tag{7}$$

The change in regenerator temperature gradient involves the change in magnitudes of w_+ and w_- with the dominant travelling wave determining the direction of the net acoustic power. To assist in the analysis, we used the reciprocal of the standing wave ratio (σ). The standing wave ratio (SWR) describes the ratio of the amplitude of a given antinode to the amplitude of an adjacent node. In effect, it also describes the degree of which the measured wave is close to being a perfect travelling wave or standing wave.

Due to the divergence of SWR when the acoustic field approaches a perfect standing wave, where $|w_+| \approx |w_-|$, we have elected to use the reciprocal of SWR (σ) in our analysis. The σ is calculated using the pressure magnitudes of w_- and w_+:

$$\sigma = \frac{1}{\mathrm{SWR}} = \frac{|w_+| - |w_-|}{|w_+| + |w_-|} \tag{8}$$

Therefore, a perfect standing wave will have a σ of 0. For a perfect travelling wave, the value of σ is -1 or 1. The sign of σ indicates which travelling wave, w_+ or w_-, is dominant or larger in magnitude.

5. Results and analysis

5.1. Configuration A

5.1.1. Positional reversal of hot and cold sections

Fig. 4 shows the temperature change of the regenerator ends T_1 and T_2 in relation to frequency using a 3 W input electric power. It has been observed that at frequencies below 230 Hz, the hot section was at the further end of the regenerator. At around 230 Hz, a switch in positions of the hot and cold sections occurs thus above this frequency, the further end of the regenerator became the cold section. The largest temperature differences obtained were at frequencies 120 Hz and 380 Hz being 11.6 K and -11.2 K respectively.

Using an input electric power of 38 W for 10 min it was possible to obtain a temperature difference of 30.9 K for 120 Hz and -31.6 K for 380 Hz. Temperature change in relation to operating time for 38 W input electric power at these two frequencies are displayed in Fig. 5.

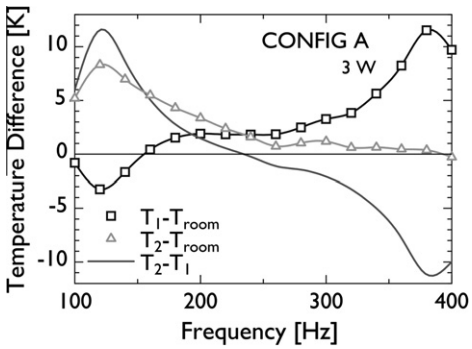

Fig. 4. Relation between frequency and temperatures recorded after 60 min run time using 3 W input electric power.

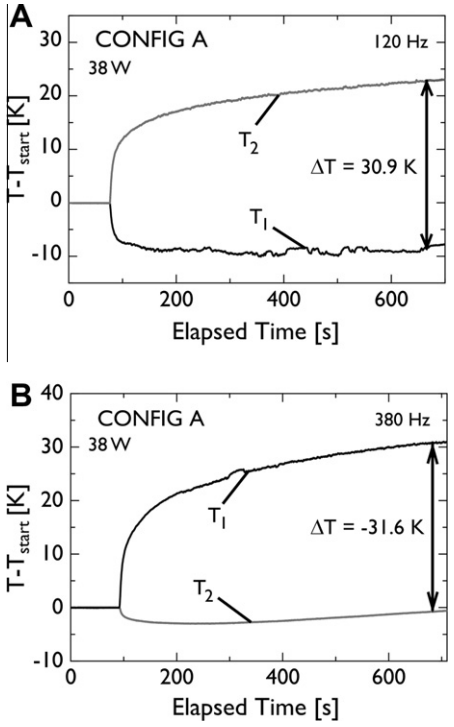

Fig. 5. Temperature of the regenerator ends using 38 W input electric power at the driver for: (A) 120 Hz and (B) 380 Hz; $\Delta T = T_2 - T_1$ displayed is after a running time of 600 sec.

5.1.2. Regenerator temperature distribution

Fig. 6 shows the change of regenerator temperature within the range of testing frequencies using 3 W input electric power for a running time of 60 min. Fig. 6A displays the regenerator temperature distribution from 100 Hz to 200 Hz. Operation at 100–160 Hz shows a linear temperature distribution, with the largest temperature gradient at 120 Hz. Departure from this optimum frequency results in a more gradual temperature gradient.

Fig. 6B shows the temperature distribution from 200 Hz to 300 Hz. At 240 Hz, we observed a U-shaped temperature distribution with the minimum temperature at the center and almost equal temperatures at both ends of the regenerator. Above 240 Hz, cold and hot sections reverse with the T_1 side becoming the hot section and the T_2 side becoming the cold section.

This U-shaped temperature distribution is of particular interest as it shows that heat is pumped from the center of the regenerator to the ends. Fig. 7 presents the U-shaped temperature distribution at 240 Hz using 38 W input electric power.

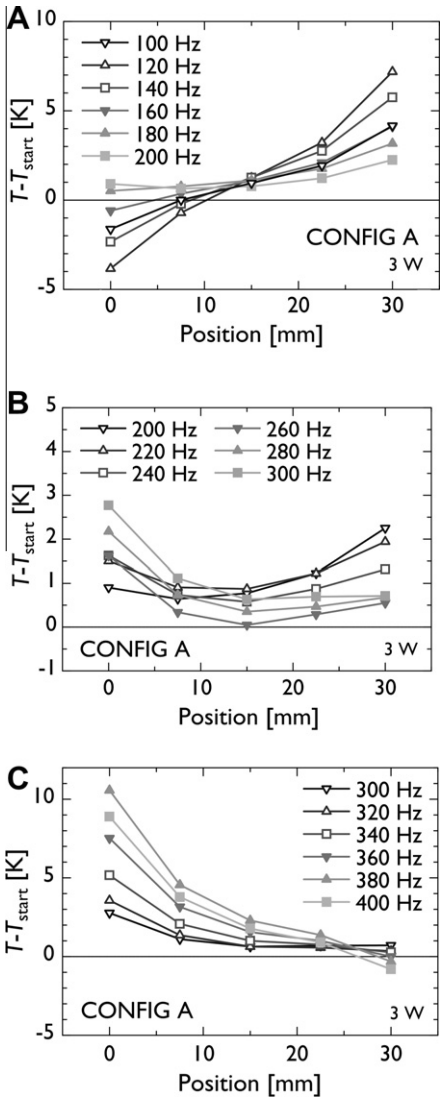

Fig. 6. Configuration A regenerator temperature distribution after 60 min using 3 W input electric power for: (A) 100 Hz $\leqslant f \leqslant$ 200 Hz, (B) 200 Hz $\leqslant f \leqslant$ 300 Hz and (C) 300 Hz $\leqslant f \leqslant$ 400 Hz; T_1 is located at $x = 0$ mm and T_2 is located at $x = 30$ mm.

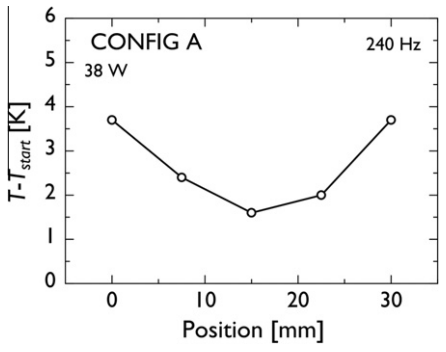

Fig. 7. Configuration A regenerator temperature distribution at 240 Hz after 10 min using 38 W input electric power; T_1 is located at $x = 0$ mm and T_2 is located at $x = 30$ mm.

As standing wave thermoacoustic effects are negligible, only travelling wave thermoacoustic effects can account for the observed phenomenon. According to thermoacoustic theory, for a travelling wave heat pump, heat is pumped opposite to the direction of the propagating travelling wave [4]: a positive direction

travelling wave will pump heat in the negative direction and a negative direction travelling wave pump heat in the positive direction. Since we have heat being pumped in both positive and negative directions, both positive and negative direction travelling waves must be considered. Therefore, as we have mentioned in Section 4, it is important to decompose the measured pressure wave into its positive (w_+) and negative (w_-) direction travelling wave components.

5.1.3. Dominant travelling wave effect on heat pumping direction

Fig. 8 shows the relationship between the σ obtained from the magnitudes of the positive ($|w_+|$) and negative direction ($|w_-|$) travelling waves within the annulus on the T_1 side of the regenerator. From Eq. (8), the sign of σ will indicate the propagating direction of the dominant travelling wave in the measured section, which in Configuration A is the annulus at the T_1 end of the regenerator. This dominant travelling wave direction will correspond to the net acoustic power within the measured section.

Examining Figs. 4 and 6, it can be seen that for frequencies of 120 Hz and 380 Hz and adjacent frequencies, σ corresponds well to the theoretical direction of heat pumping within the regenerator for a travelling wave device. At 120 Hz, the dominant travelling wave is in the negative direction (w_-), while the heat pumping is in the positive direction, as indicated by the temperature distribution given in Fig. 6A. Meanwhile at 380 Hz, the dominant travelling wave is in the positive direction (w_+) with heat pumping in the negative direction as can be seen by the temperature distribution in Fig. 6C.

The change in dominant travelling wave from w_- to w_+ occurs at around 170 Hz. From 170 Hz to 240 Hz, we can see the minimum temperature within the regenerator shift from the T_1 end to the center as displayed in Fig. 6B. This coincidence of the beginning of the shift and the change in dominant travelling wave shows that the change of dominant travelling wave direction is the cause of the change in heat pumping direction within the regenerator. The direction of heat pumping at a given end of the regenerator is therefore dependent on the dominant travelling wave, and thus the direction of net acoustic power, at that regenerator end.

In addition, the presence of a minimum temperature within the regenerator reveals that the change in heat pumping direction may occur at only a part of the regenerator and does not need to occur along the entire length of the regenerator. However, full understanding of the phenomenon is limited as Configuration A does not allow pressure measurement at the annulus on the T_2 side of the regenerator. This is addressed by Configuration B.

5.2. Configuration B

5.2.1. Regenerator temperature distribution

Fig. 9 shows the regenerator temperature distribution for frequencies 100–400 Hz using 3 W electrical input power for Configuration B. As can be seen, the change in configuration has resulted in a change in the temperature distribution relationship to frequency. The largest temperature difference at low frequency has been shifted to 100 Hz and the switch of hot and cold sections has occurs at around 170 Hz.

5.2.2. Heat pumping due to positive and negative direction travelling waves

Fig. 10 shows the values of σ on the T_1 and T_2 sides of the regenerator. At 100 Hz and 120 Hz, it can be seen that at both ends of the regenerator, the dominant travelling wave is w_-, indicated by negative values of σ. Dominant travelling waves being in the same direction on both ends of the regenerator will result in the regenerator temperature distribution being linear as the heat pumping

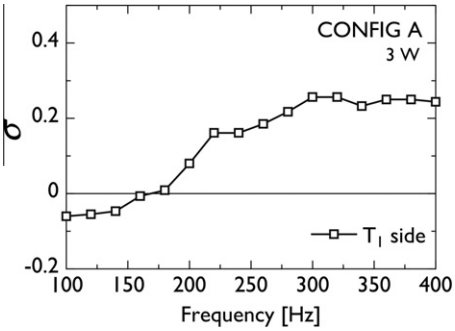

Fig. 8. Relation between the σ and frequency for Configuration A.

direction remains the same along the entire length of the regenerator.

At around 130 Hz, the dominant travelling wave on the T_1 side switches to w_+. w_+ then remains dominant at T_1 for the remainder of the tested frequency range. Similar to the observation in Configuration A, we see that this switch begins the change in heat pumping direction toward the T_1 side. Configuration A has also

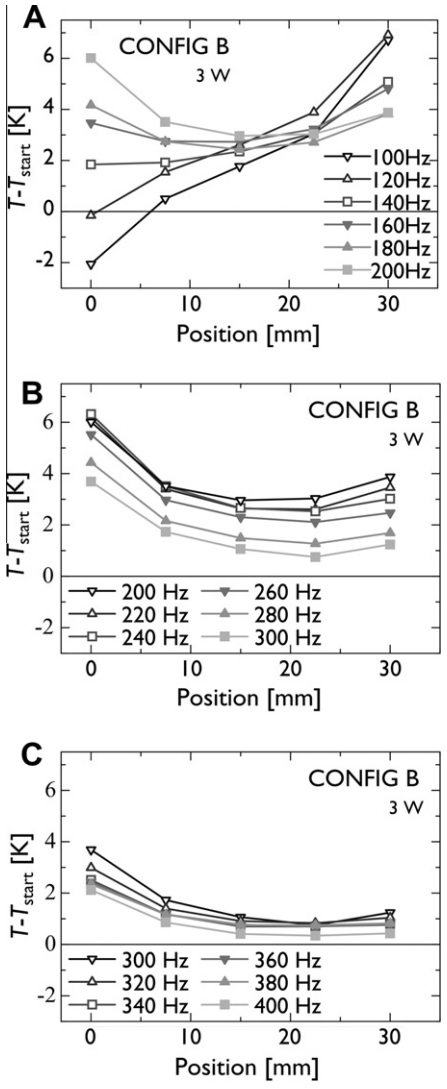

Fig. 9. Configuration B regenerator temperature distribution after 60 min using 3 W input electric power for: (A) 100 Hz $\leqslant f \leqslant$ 200 Hz, (B) 200 Hz $\leqslant f \leqslant$ 300 Hz and (C) 300 Hz $\leqslant f \leqslant$ 400 Hz; T_1 is located at x = 0 mm and T_2 is located at x = 30 mm.

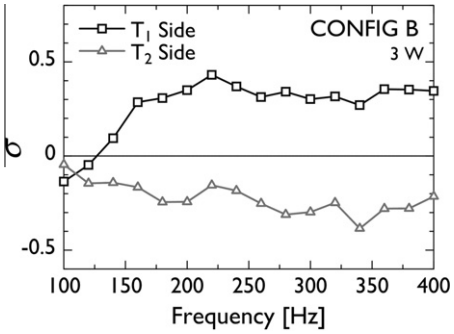

Fig. 10. Relation between σ and acoustic frequency for Configuration B.

demonstrated that the heat pumping direction at a given end of the regenerator is dependent on the direction of the dominant travelling wave at that end.

Configuration B provides added knowledge that, on the T_2 side, w_- is dominant throughout the entire tested frequency range. Therefore, above 130 Hz, we have a dominant w_+ on the T_1 side and a dominant w_- on the T_2 side and thus net acoustic power entering the regenerator from both ends. Due to this, heat is pumped in the negative direction at the T_1 side and in the positive direction at the T_2 side, ultimately resulting in the observed U-shaped temperature distribution seen in both Configuration A and B.

5.2.3. Travelling wave attenuation effects on heat pumping

The mechanism to why the magnitudes of w_+ and w_- differ between the two sides of the regenerator involves the attenuation and amplification of each individual travelling wave. As described by Ceperley [4] and demonstrated in detail by Biwa et al. [13], travelling waves passing through the regenerator will experience thermoacoustic energy conversion resulting in amplification or attenuation of the wave depending on whether it propagates against or along the temperature gradient within the regenerator. In addition, viscous losses will also influence the wave [15], which may result in attenuation even though the wave propagates along the temperature gradient.

Configuration B has allowed us to observe the change of magnitudes of both w_- and w_+ as they pass through the regenerator. Fig. 11 shows $|w_+|$ and $|w_-|$ on both sides of the regenerator for the tested frequency range. Comparing these results to Fig. 9, we can see that indeed the travelling wave that propagates against the temperature gradient experiences a reduction in magnitude, indicating attenuation.

The change of $|w_-|$ passing through the regenerator demonstrates how wave attenuation may change the dominant travelling wave and net acoustic power flow direction. At 120 Hz and below, the w_- attenuates as it passes through the regenerator as such that the exiting $|w_-|$ is still larger than the entering $|w_+|$ at the T_1 side. We therefore obtain dominant travelling waves and net acoustic power flow in the negative direction for both sides of the regenerator. Meanwhile, above 130 Hz, the dominant w_- on the T_2 side attenuates to a level below the entering w_+ on the T_1 side. This will result in a dominant w_+ on the T_1 side and thus net acoustic power flow entering the regenerator from both ends.

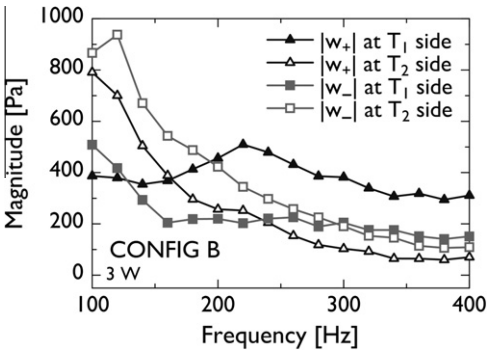

Fig. 11. $|w_+|$ and $|w_-|$ at the T_1 and T_2 sides of the regenerator at frequencies 100–400 Hz.

Also of interest is the evolution of the degree of attenuation or amplification for both $|w_-|$ and $|w_+|$ passing through the regenerator as frequency is increased from 100 Hz to 400 Hz. At 100 Hz and 120 Hz $|w_+|$ is amplified as it passes through the regenerator. As frequency is increased, $|w_+|$ is eventually attenuated and with higher frequencies the attenuation becomes more severe. The opposite occurs for $|w_-|$, which experiences severe attenuation at 100 Hz and 120 Hz. Increasing frequency will cause the attenuation to be more gradual, until above 300 Hz where $|w_-|$ is amplified.

6. Conclusion

We have constructed two coaxial travelling wave thermoacoustic heat pumps employing an annular regenerator. Experiments with frequencies ranging from 100 Hz to 400 Hz have been conducted. Within this frequency range it has been demonstrated that it is possible to alter the heat transport direction within the regenerator of a coaxial Stirling thermoacoustic heat pump using a change in frequency. This alteration of heat transport direction can be used to reverse the positions of the hot and cold sections of the regenerator.

The standing wave thermoacoustic effects have been rendered negligible by a regenerator design employing a very small $\omega\tau$. Therefore, the observed thermoacoustic effect is only due to travelling waves. As the acoustic field consists of positive and negative direction travelling waves, it is important to decompose the measured pressure wave into its w_+ and w_- components. We have discovered that both travelling waves, the positive direction travelling wave (w_+) and negative direction (w_-) travelling wave influence the temperature distribution within the regenerator. The dominant travelling wave at a given section of the regenerator will determine the direction of heat pumping at that section.

The magnitudes of the exiting w_+ and w_- are influenced by the attenuation or amplification within the regenerator. Attenuation may yield an exiting w_- being reduced to a magnitude lower than the entering w_+, thus yielding a net acoustic power flowing into the regenerator from both ends. Heat will therefore be pumped towards both ends of the regenerator and resulting in a minimum regenerator temperature located within the regenerator. As the location of this minimum temperature may shift, the reverse in heat pumping direction does not have to occur along the entire length of the regenerator and may occur only within a part of the regenerator.

However, at the moment, the relationship between the magnitudes of w_+ and w_- and the exact position of the minimum temperature within the regenerator is still unclear. In addition, the relationship between the value of $|\sigma|$ to the performance has not been explained. A more elaborate mathematical treatment of this phenomenon is planned for future work.

The ability to create a frequency dependent hot/cold section reversal has tremendous potential and increases the significance of the coaxial Stirling thermoacoustic heat pump design. It will allow heating and cooling, using a single device without additional specialized parts. Future applied devices such as thermoacoustic cryocooler using the coaxial configuration will be able to switch operation from a cryocooler to a superheater and vice versa by a mere change in operating frequency.

Acknowledgements

We would like to express our deepest gratitude to Professor Tetsushi Biwa of Tohoku University for his valuable advice and discussion regarding the coaxial configuration of the travelling wave thermoacoustic devices. The utmost appreciation also goes to Mr. Sumitomo Hidaka and Mr. Takeshi Matoba of the Thermal Engineering Labs of Kyushu University for assisting us with the machining and fabrication of the coaxial thermoacoustic device.

References

[1] Swift GW. Thermoacoustic engines. J Acoust Soc Am 1988;84:1145–80.
[2] Tijani MEH, Zeegers JCH, de Waele ATAM. Design of thermoacoustic refrigerators. Cryogenics 2002;42:49–57.
[3] Wheatley J, Hofler T, Swift GW, Migliori A. Understanding some simple phenomena in thermoacoustics with applications to acoustical heat engines. Am J Phys 1985;53:147–62.
[4] Ceperley PH. A pistonless Stirling engine – the traveling heat wave engine. J Acoust Soc Am 1979;66:1508–13.
[5] Yazaki T, Iwata A, Maekawa T, Tominaga A. Traveling wave thermoacoustic engine in a looped tube. Phys Rev Lett 1998;81:3128–31.
[6] Backhaus S, Swift GW. A thermoacoustic-Stirling heat engine: detailed study. J Acoust Soc Am 2000;107:3148–66.
[7] Yazaki T, Biwa T, Tominaga A. A pistonless Stirling cooler. Appl Phys Lett 2002;80.
[8] Poese ME, Smith RWM, Garrett SL, Gerwen Rv, Gosselin P. Thermoacoustic refrigeration for ice cream sales. In: Proceedings of the 6th IIR Gustav Lorentzen conference; 2004.
[9] Tijani MEH, Spoelstra S. Study of a coaxial thermoacoustic-Stirling cooler. Cryogenics 2008;48:77–82.
[10] Biwa T, Morii J. Acoustic field measurement of a coaxial thermoacoustic cooler. In: 13th Stirling cycle symposium, Tokyo; 2010.
[11] Kang H, Zhou G, Li Q. Thermoacoustic effect of traveling-standing wave. Cryogenics 2010;50:450–8.
[12] Biwa T, Tashiro Y, Yazaki T. How does Stirling engine work? J Power Energy Syst 2008;2:1254–60.
[13] Biwa T, Tashiro Y, Mizutani U, Kozuka M, Yazaki T. Experimental demonstration of thermoacoustic energy conversion in a resonator. Phys Rev E 2004;69.
[14] Bucher I. Estimating the ratio between travelling and standing vibration waves under non-stationary conditions. J Sound Vib 2004;270:341–59.
[15] Swift GW. Thermoacoustics: a unifying perspective for some engines and refrigerators. Melville, NY: Acoustical Society of America; 2002.